



**The influence of surface  $\text{CO}_{\text{2}}$  condensation on the evolution of warm and cold rocky planets orbiting Sun-like stars**

Journal:	<i>Monthly Notices of the Royal Astronomical Society</i>
Manuscript ID	Draft
Manuscript type:	Main Journal
Date Submitted by the Author:	n/a
Complete List of Authors:	Bonati, Irene; Tokyo Institute of Technology Earth Life Science Institute Ramirez, Ramses; Tokyo Institute of Technology, Earth-Life Science Institute
Keywords:	planets and satellites: terrestrial planets < Planetary Systems, planets and satellites: atmospheres < Planetary Systems, planets and satellites: physical evolution < Planetary Systems

SCHOLARONE™  
Manuscripts

# The influence of surface $CO_2$ condensation on the evolution of warm and cold rocky planets orbiting Sun-like stars

I. Bonati,<sup>1</sup><sup>★</sup> R. M. Ramirez,<sup>1,2</sup>

<sup>1</sup>*Earth-Life Science Institute, Tokyo Institute of Technology, Tokyo, Japan*

<sup>2</sup>*Space Science Institute, Boulder, Colorado, USA*

Accepted XXX. Received YYY; in original form ZZZ

## ABSTRACT

The habitable zone is the region around a star where standing bodies of liquid water are stable on a planetary surface. Its width is dictated by the efficiency of the carbonate-silicate cycle, which has maintained habitable surface conditions on our planet for billions of years. This cycle may be severely inhibited by significant surface condensation of  $CO_2$  ice, which is likely to occur on distant planets containing high enough levels of atmospheric  $CO_2$ . Such a process could permanently trap  $CO_2$  ice within the planet, diminishing its long-term habitability. Recent work has modeled this scenario for initially cold and icy planetary bodies orbiting our Sun. Here, we use an advanced energy balance model to consider both initially warm and cold rapidly-rotating planets orbiting F - K stars. We show that the range of orbital distances where significant surface  $CO_2$  ice condensation occurs is significantly reduced for warm start planets. Star type does not affect this conclusion, although surface  $CO_2$  ice condenses over a larger fraction of the habitable zone around hotter stars. Our warm start simulations are thus consistent with 1-D model predictions, suggesting that the size of the classical  $CO_2$ - $H_2O$  habitable zone in those earlier models are still valid. We also find that our cold start simulations exhibit trends that are consistent with those of previous work.

**Key words:** planets and satellites: terrestrial planets – planets and satellites: atmosphere – planets and satellites: physical evolution

## 1 INTRODUCTION

During the course of its evolution, Earth is thought to have exhibited mostly warm surface conditions that were temporarily interrupted by a few sporadic cooling episodes, triggered by processes taking place in its interior, atmosphere, and host star. The resultant climatic changes can manifest as mild oscillations, or even as extreme snowball events (Kirschvink 1992; Hoffman et al. 1998), with Earth’s surface being completely covered in ice. Nevertheless, the carbonate-silicate cycle, which maintains the balance of atmospheric  $CO_2$  between the atmosphere and the interior, has allowed Earth to escape permanent glaciation and maintain clement surface conditions throughout time (Hoffman et al. 1998).

However, large amounts of atmospheric  $CO_2$  on a cold enough planet, like is the case for some depictions of early Mars (Kasting 1991; Wordsworth et al. 2013), can have a detrimental effect on its habitability. A number of recent studies (Kasting 1991; Pierrehumbert 2005; Pierrehumbert et al. 2011; Soto et al. 2015; Turbet et al. 2017) have shown that once  $CO_2$  partial pressures exceed the saturation level, and temperatures are low enough, significant condensation occurs at the poles, triggering collapse (Figure 1).

The relatively high Rayleigh scattering of  $CO_2$ , and the resultant increase in the planetary albedo, further enhance the ice-albedo feedback (Kasting 1991) and keep the planet cold. Moreover, the high density of  $CO_2$  ice with respect to water ice can lead to subsurface sequestration of the former, removing it from the atmosphere forever, resulting in a permanent state of glaciation. Such a scenario potentially removes or greatly mitigates the role of the carbonate-silicate cycle in sustaining habitable surface conditions (Turbet et al. 2017).

Thus, while the carbonate-silicate cycle has stabilized surface temperatures over time on Earth, this might not be the case for bodies orbiting other stars and/or located at different orbital distances, and having different atmospheric  $CO_2$  inventories. In particular,  $CO_2$  pressures at large orbital distances are high enough for surface condensation and Rayleigh scattering to counter the greenhouse effect, directly impacting the width of the classical  $CO_2$ - $H_2O$  habitable zone (Kasting et al. 1993; Kopparapu et al. 2013; Ramirez 2018).

It is therefore important to assess the role of  $CO_2$  in determining a given planet’s fate. Turbet et al. (2017) have recently addressed this issue by using a 3-D Global Climate Model (GCM) to simulate the evolution of terrestrial planets across the habitable zone, and concluded that bodies remained fully frozen and exhibited permanent surface  $CO_2$  ice condensation at orbital distances as small as

\* E-mail: irene.bonati@elsi.jp (IB)

## 2 I. Bonati and R. Ramirez

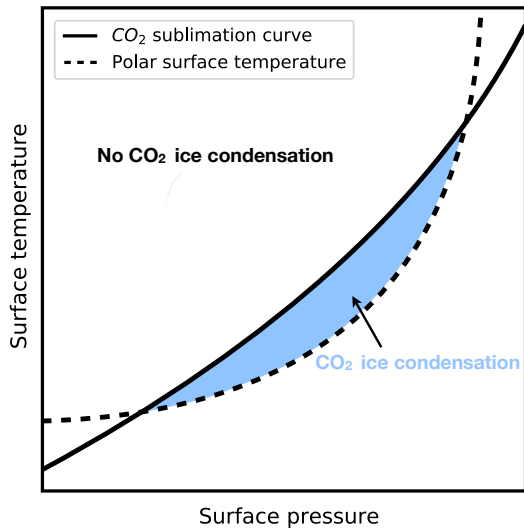


**Figure 1.** Schematic representation showing the  $CO_2$  sublimation and the polar surface temperature curves as a function of surface temperature and pressure. At the poles, the surface temperature is low enough to drop below the  $CO_2$  sublimation temperature. The presence of a sufficiently high amount of atmospheric  $CO_2$  can, in turn, drive precipitation of  $CO_2$  ice onto the planetary surface. Such a phenomenon does not happen for low contents of  $CO_2$ , or when the warming effect of  $CO_2$  starts dominating at high surface pressures. Adapted from Figure 1 of Soto et al. (2015).

~1.27 AU from the Sun for an atmospheric  $CO_2$  pressure of 1 bar. In comparison, 1-D calculations suggest that planets can remain habitable up to ~1.47 AU at that  $CO_2$  pressure level (Kasting et al. 1993; Kopparapu et al. 2013; Ramirez 2018). All of this suggests that  $CO_2$  condensation in more advanced climate modeling simulations may have an even more detrimental effect on planetary habitability than previously calculated, possibly decreasing the size of the habitable zone as computed in 1-D models.

However, Turbet et al. (2017) had simulated planets with initially fully-glaciated surface conditions (cold start worlds) orbiting our Sun. In contrast, habitable zone planets that start their evolution warm (warm start worlds) may exhibit different responses to  $CO_2$  condensation. Here, we employ an advanced energy balance model (EBM) to investigate the parameter space of surface  $CO_2$  condensation for cold and warm rotating planets with different atmospheric  $CO_2$  pressures orbiting Sun-like (F - K) stars. We compare the cold and warm start results and discuss the implications for the width of the habitable zone.

## 2 METHODS

### 2.1 Governing equations

We make use of an advanced non-grey energy balance model (EBM), similar to that described in Ramirez & Levi (2018) and Ramirez (2020), which is itself based on other similar models (see also North & Coakley Jr (1979), North et al. (1981), Williams & Kasting (1997), and Vladilo et al. (2013)) to determine the presence of  $CO_2$  ice condensation and its influence on the fate of bodies orbiting Sun-like stars. We study the evolution of Earth-like planets assuming cold ( $T_{\text{surf}}=230$  K) or warm ( $T_{\text{surf}}=280$  K) starts. The EBM is coupled to a 1-D radiative-convective climate model that provides the radiative transfer calculations. For a more detailed explanation of the model, the reader is redirected to Ramirez (2020).

The present model follows the radiative energy balance principle (e.g., Williams & Kasting 1997), according to which planets in thermal equilibrium radiate as much energy to space as they receive from their host star. The atmospheric-ocean energy balance is expressed as (e.g., James & North 1982; Williams & Kasting 1997):

$$C_p \frac{\partial T(x,t)}{\partial t} - \frac{\partial}{\partial x} D (1 - x^2) \frac{\partial T(x,t)}{\partial x} + I - L \left( \frac{dM_{\text{col},CO_2}}{dt} \right) = S(1-A), \quad (1)$$

where  $C_p$  is the effective heat capacity,  $T$  is the zonally averaged surface temperature,  $x$  is the sine of the latitude,  $t$  is time,  $D$  is the heat diffusion coefficient (i.e., the latitudinal transport of heat),  $I$  is the outgoing infrared flux to space,  $S$  is the absorbed fraction of incident solar flux,  $L$  is the latent heat flux per unit mass of  $CO_2$  ( $5.9 \times 10^5$  J/kg; Forget et al. (1998)),  $M_{\text{col},CO_2}$  is the column mass of  $CO_2$  which sublimates from or condenses onto the planetary surface, and  $A$  is the albedo at the top of the atmosphere over a given time step. This equation is solved for every time step using a second-order finite difference scheme.

The modeled planets are Earth-sized and are subdivided into  $36 5^\circ$  wide latitudinal belts with land and ocean coverage similar to present-day Earth (i.e., 70% oceans and 30% land). Flat topography is assumed for simplicity. Planets are in circular orbits and a day is 24 hours. For the calculations, we assume that atmospheres are fully-saturated and consist of 1 bar  $N_2$  for a range of atmospheric  $CO_2$  pressures. The thermal diffusion coefficient  $D$  is calculated using the following scaling relation (with the subscript "0" referring to present Earth values):

$$\left( \frac{D}{D_0} \right) = \left( \frac{p}{p_0} \right) \left( \frac{C_p}{C_{p0}} \right) \left( \frac{m_0}{m} \right)^2 \left( \frac{\Omega_0}{\Omega} \right)^2 \left( \frac{T_{\text{surf,ave}}}{T_0} \right)^{12}, \quad (2)$$

where  $D_0 = 0.58 \text{ W m}^{-2} \text{ K}^{-1}$ ,  $C_{p0} = 10^3 \text{ g}^{-1} \text{ kg K}^{-1}$ ,  $p$  is the atmospheric pressure ( $p_0 = 1$  bar),  $m$  is the atmospheric mass ( $m_0 = 28 \text{ kg}$ ),  $\Omega$  is the planetary rotation rate ( $\Omega_0 = 7.27 \cdot 10^{-5} \text{ rads}^{-1}$ ), and  $T_{\text{surf,ave}}$  is the annual average surface temperature ( $T_0 = 288 \text{ K}$ ). A crude temperature dependence is added to this equation to simulate the importance of latent heat release and transport at high temperatures (Caballero & Langen 2005; Rose et al. 2017). The exponent 12 on the right side of Equation 2 gives the right latitudinal temperature structure when comparing our results to Figure 1 from Turbet et al. (2017), which displays an average temperature  $T_{\text{surf,ave}} \sim 225 \text{ K}$ . Without this temperature dependence, equator-pole temperature gradients are underestimated and heat transport is overestimated at cold temperatures.

The model is able to distinguish between land, ocean, ice, and clouds. As the atmosphere warms near and above the freezing point, water clouds form, with the latitudinal cloud coverage ( $c$ ) dictated by:

$$c = \min \left( 0.72 \log \left( \frac{F_C}{F_E} + 1 \right), 1 \right). \quad (3)$$

Here,  $F_C$  is the convective heat flux,  $F_E$  is the convective heat flux for the Earth at 288 K ( $\sim 90 \text{ W/m}^2$ ). This equation is similar to that used in the Community Atmosphere Model (CAM) GCM (Xu & Krueger 1991; Yang & Abbot 2014) and yields an Earth-like cloud cover ( $c$ ) of  $\sim 50\%$  at a mean surface temperature  $T_{\text{surf}} = 288 \text{ K}$ .

For each time step, spanning about 2 hours of a planet's evolution, the new average surface temperature is updated for every latitude belt following Equation 1, along with the resulting  $H_2O$

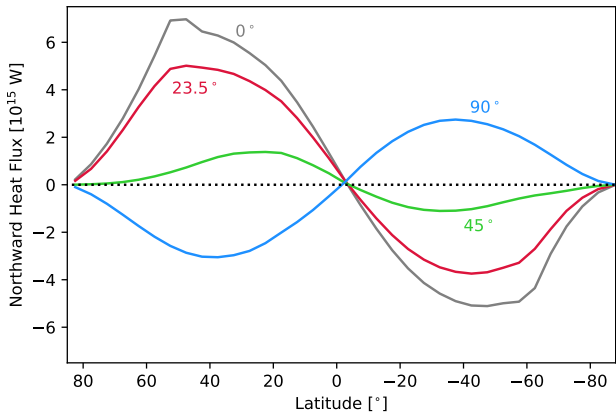


**Figure 2.** Meridional heat flow for an Earth-like planet orbiting a Sun-like star at 1 AU, having an atmospheric pressure of  $CO_2$  of  $3.3 \cdot 10^{-4}$  bar and obliquities  $0^\circ$ ,  $23.5^\circ$ ,  $45^\circ$ , and  $90^\circ$ . At low obliquities, heat is transported from the equator towards the poles, while transport in the opposite direction is favored at high enough obliquities.

and  $CO_2$  inventories in the atmosphere and surface. The model simulates the entire year, including seasons, until convergence (i.e., until the average annual surface temperature does not change by more than  $\sim 0.1$  K) using an explicit forward marching numerical scheme.

To validate our model, we compute the northward heat flux for a planet with 330 ppm  $CO_2$  (i.e., similar to present Earth) and orbiting the Sun at 1 AU at different obliquities by using the following expression:

$$\mathcal{F}_\lambda = 2\pi R \cos \lambda F_\lambda = 2\pi R^2 D \cos^2 \lambda \frac{\partial T}{\partial x}, \quad (4)$$

where  $\mathcal{F}_\lambda$  is the latitudinal energy transport per unit length,  $R$  is the planetary radius,  $\lambda$  is the latitude (between  $-90^\circ$  and  $90^\circ$ ), and  $\frac{\partial T}{\partial x}$  is the temperature gradient between different latitude belts. The obtained flux, shown in Figure 2, matches well with similar models used in past studies (e.g., Williams & Pollard 2003).

## 2.2 Initial conditions and parameter space

We model the evolution of Earth-sized bodies, orbiting F0, K5, and solar (a G2) stars. We vary the initial  $CO_2$  atmospheric pressure, surface temperature (cold and warm start), planetary obliquity, and semi-major axis. The initial conditions are summarized in Table 1. If a planet starts out cold, there are no water clouds (initially) in the atmosphere. The global surface temperature is set to  $T_{\text{surf}} = 230$  K, and the land snow fraction is equal to 1 (i.e., the continents are fully covered in ice).

On the other hand, if a planet starts out warm, the surface temperature is set to  $T_{\text{surf}} = 280$  K, with a land snow fraction of 0.5. The fractional cloud cover from water vapor is  $c_{H_2O} = 0.26$  (resulting from Equation 1). There are no  $CO_2$  clouds in the initial step for either case (i.e.,  $c_{CO_2} = 0$ ). These starting conditions are meant to approximately simulate the modeling conditions of Turbet et al. (2017). However, after the initial step, both cloud coverage and surface temperatures are self-consistently calculated.

Our modeled  $CO_2$  clouds are non-absorbing, and thus radiatively inactive. This is consistent with recent simulations suggesting that their greenhouse effect may be very small in these dense  $CO_2$

**Table 1.** Initial conditions for planets starting out cold and warm.

Parameter	Cold start	Warm start
Surface temperature $T_{\text{surf}}$ [K]	230	280
$H_2O$ cloud fraction $c_{H_2O}$	0	0.26
$CO_2$ cloud fraction $c_{CO_2}$	0	0
Land snow fraction	1	0.5

**Table 2.** Parameter space investigated in the simulations.

Parameter	Values		
$CO_2$ partial pressure range [bar]	0.01-3.0		
Obliquity [°]	0, 23.5		
Stellar Temperature [K]	F0 star 7200	Sun 5800	K5 star 4400
Stellar mass [ $M_\odot$ ]	1.5	1.0	0.6
Stellar luminosity [ $L_\odot$ ]	4.3	1.0	0.15
Semi-major axis range [AU]	2.0-3.0	1.0-1.5	0.4-0.6

atmospheres (Kitzmann 2016). Even so, our  $CO_2$  clouds still impact the planetary albedo, affecting planetary surface temperatures and  $CO_2$  precipitation. Following GCM predictions (Forget et al. 2013), a 50 percent cloud cover is assumed for  $CO_2$  clouds forming within a given latitude band.

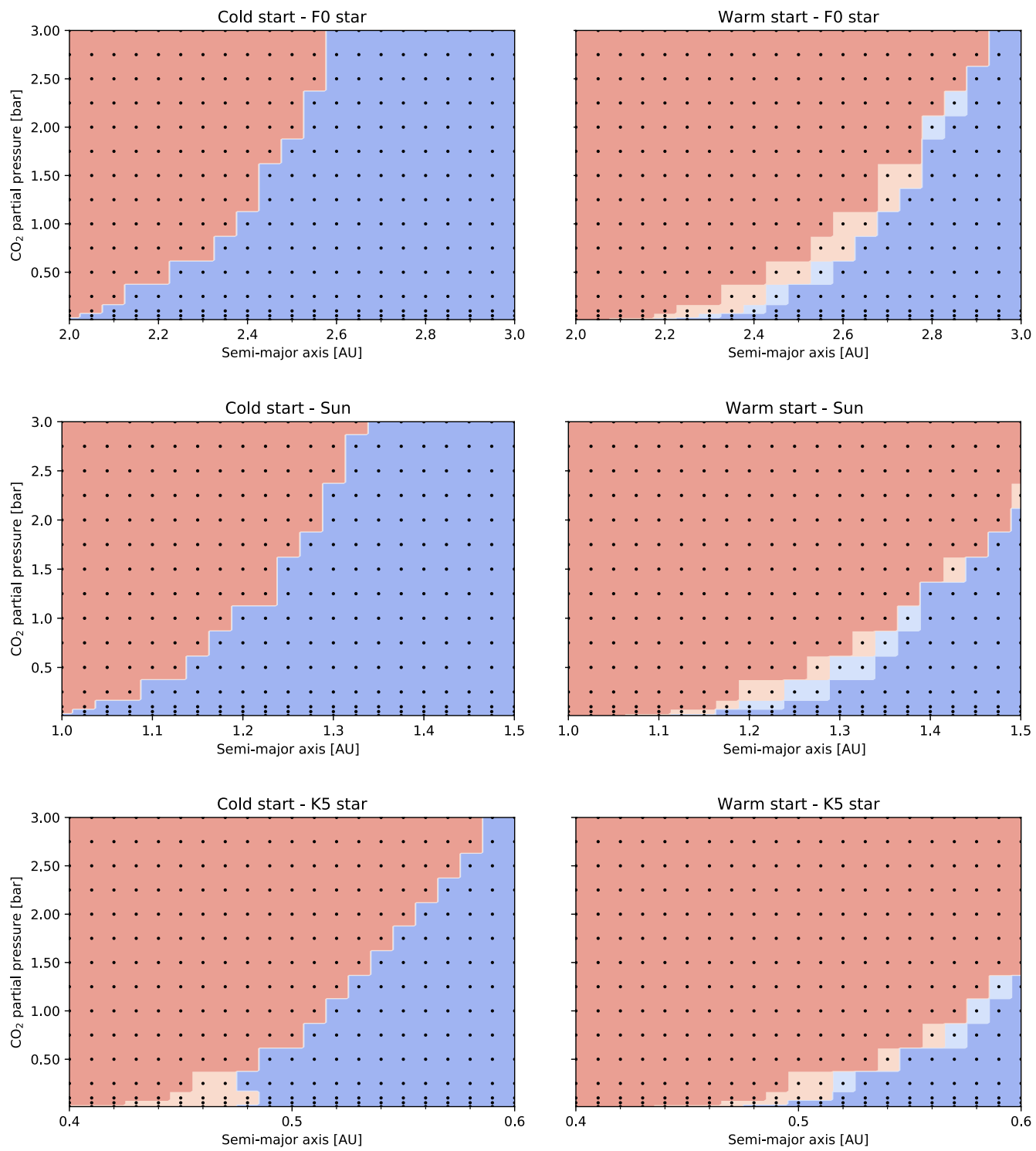
We explore different parameters as shown in Table 2. We do not simulate planets located at larger semi-major axis distances than those showed in Table 2 because modeled surface temperatures at these  $CO_2$  pressures are below what is possible for our radiative transfer model ( $T_{\text{surf}} = 150$  K). Nevertheless, the sampled parameter space is more than sufficient to obtain the overall trends.

## 3 RESULTS

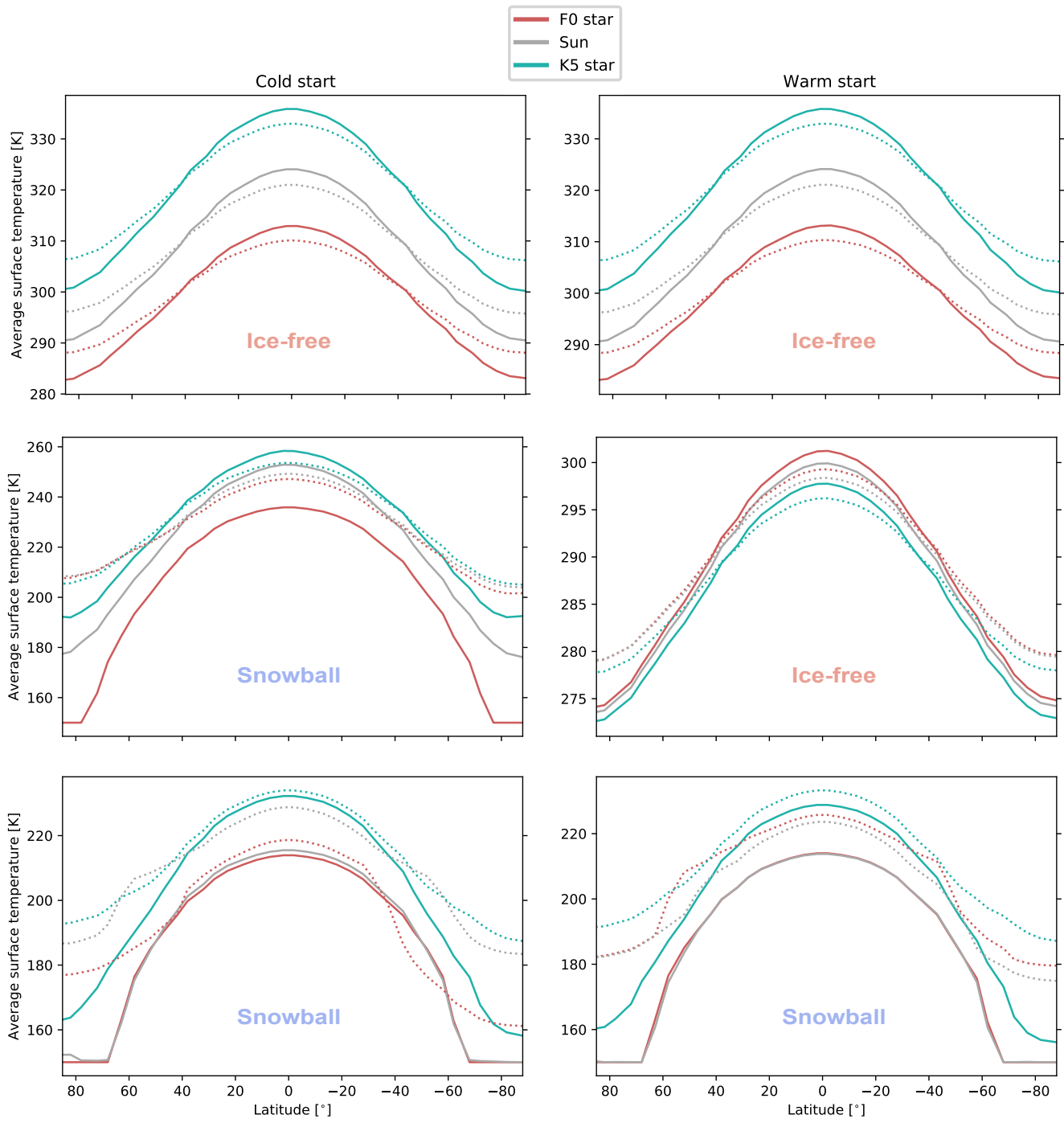
### 3.1 Steady-state climate regimes

Figure 3 shows the steady-state climate regimes obtained for initially cold and warm Earth-sized bodies with obliquity  $23.5^\circ$  orbiting different types of stars (Sun-like, as well as F0 and K5 stars), as a function of their orbital distance and the initial atmospheric pressure of  $CO_2$ . We distinguish between four final scenarios: In the first one, the planet is completely ice-free (dark red areas in Figure 3). In the second one, the planet is partially covered in  $H_2O$  ice (light red areas in Figure 3). In the third one, the planet is partially covered in both  $H_2O$  ice and (permanent)  $CO_2$  ice at the poles (light blue areas in Figure 3). In the last one, the planet is fully ice-covered and permanent  $CO_2$  ice is present on the planetary surface (blue areas in Figure 3). Permanent  $CO_2$  ice forms when condensation fluxes during the winter months do not balance sublimation taking place in the summer.

As expected, surface  $CO_2$  ice condensation occurs at smaller orbital distances for cold start planets (left panels in Figure 3) compared to bodies starting out warm (right panels in Figure 3). For the solar case, the 1 bar  $CO_2$  cold start scenario exhibits surface  $CO_2$  ice condensation starting from orbital distances as small as  $\sim 1.2$  AU, which compares favorably to the 1.27 AU value found by Turbet et al. (2017). The equivalent distances for the F0 and K5 stars are  $\sim 2.4$  AU and  $\sim 0.52$  AU, respectively. In contrast, surface  $CO_2$  ice condensation for warm starts does not occur until  $\sim 1.38$  AU for the 1 bar  $CO_2$  solar case, almost 0.2 AU farther out than for

4 *I. Bonati and R. Ramirez*

**Figure 3.** Steady-state solutions reached by warm and cold start (fully-glaciated body) planets orbiting F0, Sun-like and K5-type stars for a range of semi-major axes and initial partial pressures of atmospheric  $\text{CO}_2$ . The modeled planets have an Earth-like continental fraction and an obliquity of  $23.5^\circ$ . The dark and light red regions comprise bodies that are ice-free and partially covered in  $\text{H}_2\text{O}$  ice, respectively. The light and dark blue regions represent partially ice-covered and snowball planets displaying permanent  $\text{CO}_2$  ice on their surfaces, respectively. Note: The horizontal scale is different for each host star. Our model predicts similar trends at  $0^\circ$  obliquity (not shown).



**Figure 4.** Average surface temperature at the last time step as a function of latitude for cold start (initial  $T_{\text{surf}} = 230$  K; left column) and warm start (initial  $T_{\text{surf}} = 280$  K; right column) bodies having an initial atmospheric CO<sub>2</sub> pressure of 1 bar. Each row samples a different region of the diagrams shown in Figure 3, for planets having obliquities of both 0° (solid lines) and 23.5° (dashed lines). The colors differentiate between planets orbiting F0, K5, and Sun-like stars at semi-major axes of 2.2 AU (F0 star), 1.1 AU (Sun), and 0.45 AU (K5 star; first row), 2.4 AU (F0 star), 1.25 AU (Sun), and 0.53 AU (K5 star; second row), and 2.75 AU (F0 star), 1.4 AU (Sun), and 0.6 AU (K5 star; third row). The colored text in each panel indicates the final state of all bodies contained in it (ice-free or snowball planets).

the cold start scenario. At this same pressure level, CO<sub>2</sub> surface ice starts forming at  $\sim 2.7$  AU and  $\sim 0.58$  AU for the F0 and K5 stars, respectively. This is about 0.03 AU and 0.06 AU farther out than for the equivalent cold start cases. The distances beyond which surface CO<sub>2</sub> ice condensation starts forming are pressure-dependent, as a

result of the greenhouse effect exerted by CO<sub>2</sub>. At higher pressures, surface CO<sub>2</sub> ice condensation in both warm and cold start cases occurs farther away from the host star, whereas the opposite takes place at lower pressures.

Moreover, the surface CO<sub>2</sub> ice condensation encompasses a

## 6 I. Bonati and R. Ramirez

larger region for the hotter stars (alternatively, the red region is larger for cooler stars). This is because near-infrared absorption is lower and Rayleigh scattering is higher for planetary atmospheres orbiting hotter stars, cooling the planet and causing  $CO_2$  surface ice condensation to occur closer to the star. For comparison, 1-D radiative-convective climate modeling simulations predict that planets with a 1 bar  $CO_2$  atmosphere orbiting F0, solar, and K5 stars can remain habitable at distances as far as  $\sim 2.75$ ,  $1.47$ , and  $0.58$  AU, respectively (Kasting et al. 1993; Kopparapu et al. 2013; Ramirez 2018), assuming the luminosity values given in Table 2. These values are only slightly farther out than the most distant extent of the red regions at the 1 bar level (Figure 3). Although nearly the same size, the warm regions in the warm stars still span slightly smaller areas (generally) than predicted in 1-D radiative-convective climate modeling simulations (Kasting et al. 1993; Kopparapu et al. 2013; Ramirez 2018). This is because of the EBM's increased ice-albedo feedback.

A key observation from our cold starts is that a planet cannot escape full glaciation for orbital distances exceeding  $\sim 2.55$  AU,  $\sim 1.33$  AU, and  $\sim 0.58$  AU for the F0, solar, and K5 star cold start scenarios (Figure 3). In these cases, the planet remains glaciated with surface  $CO_2$  ice condensation regardless of the atmospheric  $CO_2$  content (Figure 3). This difference is attributed to the weaker heat transport and higher surface albedo associated with such cold starts. Although Turbet et al. (2017) does not necessarily obtain  $CO_2$  surface ice in all of these cases, in agreement with our model, they predict snowball states.

### 32 3.2 Latitudinal variation of surface temperature

The average surface temperature at the last time step as a function of latitude is illustrated in Figure 4, for both initially cold and warm planets having 1 bar of  $CO_2$  in their atmospheres and obliquities  $23.5^\circ$  and  $0^\circ$ . Low obliquity bodies receive more direct insulation at the equator, which causes large temperature differences between the latter and the poles, as well as generally lower polar surface temperatures. This also produced the tendency for equatorial surface temperatures to be higher at  $0^\circ$  compared to  $23.5^\circ$  obliquity, especially at higher  $CO_2$  pressures. This, in turn, would cause more surface  $CO_2$  ice to be present at higher ( $23.5^\circ$ ) obliquity (see Figure 5).

We also find that the final state of a planet (i.e., whether it ends up being ice-free, partially ice-covered or a snowball) is not greatly influenced by obliquity variations for these dense  $CO_2$  atmospheres that are located near or very far away from their host stars (first and last rows in Figure 4). This is because at these distances, either the ice-albedo feedback (at farther distances) or the greenhouse effect (at closer distances) outstrip the impact of obliquity variations. This trend holds true whether the planet has a cold or warm start (Figure 4). However, at intermediate orbital distances (second row in Figure 4), close to the interface between the red and the blue regions (Figure 3), obliquity variations have a bigger impact on the final state.

### 56 3.3 Fraction of surface $CO_2$ ice

As shown by the Mars simulations of Soto et al. (2015), the fraction of atmospheric  $CO_2$  that condenses onto the surface depends heavily on the atmospheric  $CO_2$  pressure and the planetary obliquity. Consistent with that study, we generally find that the amount of condensed  $CO_2$  ice (i.e., the fraction of initial atmospheric  $CO_2$  that

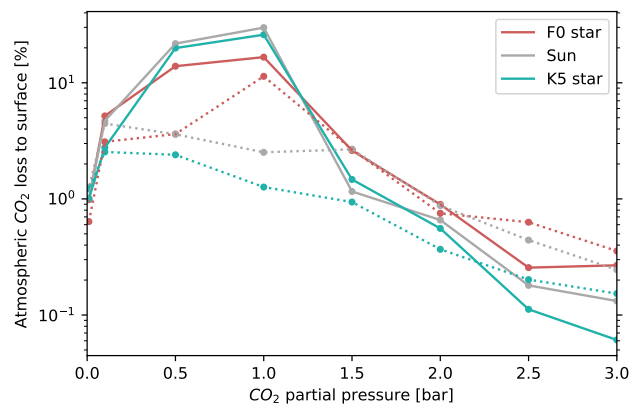


**Figure 5.** Global accumulation of  $CO_2$  ice for a range of initial atmospheric  $CO_2$  pressures for cold start ( $T_{\text{surf}} = 230$  K) bodies of  $0^\circ$  (solid lines) and  $23.5^\circ$  (dashed lines) obliquity orbiting F0, K5, and Sun-like stars at distances of  $2.75$ ,  $0.6$ , and  $1.4$  AU (same orbital distances as in the third row of Figure 4), respectively. The atmospheric  $CO_2$  ice loss to surface is defined as the portion of initial  $CO_2$  in the atmosphere that precipitates and gets trapped as permanent  $CO_2$  ice on the planetary surface.

precipitates onto the planetary surface) is highest at low obliquity ( $0^\circ$ ) and at low/intermediate pressures (Figure 5). Such a trend is expected because equator-pole transport is relatively weak at low obliquities and pressures, which favors  $CO_2$  ice condensation at the poles.

At very low atmospheric  $CO_2$  pressures (i.e., smaller than 0.1 bar), saturation is hardly ever reached, and even if the planetary surface is cold enough,  $CO_2$  will not precipitate or precipitate in very low amounts (Figure 5). Similarly, at high enough atmospheric  $CO_2$  pressures (above 2 bar) the greenhouse effect dominates and inhibits surface ice condensation, especially at lower latitudes. Under these conditions  $CO_2$  ice condensation becomes marginal (< 1 percent atmospheric  $CO_2$ ) at both obliquities (Figure 5), consistent with trends that were also found in Soto et al. (2015). For pressures higher than  $\sim 2$  bar surface  $CO_2$  condensation is slightly larger at higher ( $23.5^\circ$ ) obliquity (Figure 5). We attribute this to slightly less efficient equator-pole transport at higher obliquity for the highest pressures.

## 4 DISCUSSION

### 4.1 Implications for planetary habitability on early Mars, Earth, and exoplanets

In agreement with Turbet et al. (2017), our model also finds that  $CO_2$  surface condensation can be a detriment to the habitability of cold start planets (Figure 3). As the dense surface  $CO_2$  ice becomes sequestered within the subsurface, the atmospheric  $CO_2$  pressure decreases, which promotes even more ice formation, possibly leading to atmospheric collapse (Turbet et al. 2017). Unlike Earth, where volcanism ended snowball episodes (Hoffman et al. 1998), it might be more difficult for distant cold planets to avoid permanently glaciated conditions. This is because once  $CO_2$  pressures exceed saturation,  $CO_2$  is increasingly removed from the atmosphere before temperatures ever become warm enough. An exception to this could be volcanism rich in  $H_2$  or  $CH_4$ , which could produce sufficient  $CO_2$ - $H_2$  or  $CO_2$ - $CH_4$  collision-induced absorption at high enough concentrations (percent level) and  $CO_2$  pressures (Ramirez

et al. 2014; Ramirez & Kaltenegger 2017, 2018). Nevertheless, cold start planets that are close enough to their stars receive enough energy to circumvent the above problems (Figure 3).

The above has a couple of interesting implications. Some studies argue that Mars (located at 1.52 AU) was a cold planet that had undergone numerous transient warming episodes over geologic timescales, possibly aided by supplementary volcanic gases or other mechanisms in a predominantly  $CO_2$  atmosphere (Wordsworth et al. 2013; Batalha et al. 2016). However, multiple sporadic warming episodes would be very difficult to achieve in practice because the excess  $CO_2$  will be removed from the atmosphere once a warm period ends. This will not only enhance the ice-albedo feedback, raising the planetary albedo and triggering atmospheric collapse, but the atmospheric  $CO_2$  would be gradually removed from the atmospheric-surface system forever as it sinks below the less dense  $H_2O$  ice, making subsequent transient warming episodes much less likely.

In contrast to our cold start cases, our warm start simulations suggest that the condensation of surface  $CO_2$  ice affects a much smaller range of orbital distances. Irrespective of the star type, the range of semi-major axes and  $CO_2$  pressures for which planets exhibit habitable surface conditions is similar to that predicted by 1-D calculations of the habitable zone (Kasting et al. 1993; Ramirez 2018). That said, warm start cases that are distant enough to exhibit significant  $CO_2$  condensation suffer the same habitability problems discussed above for cold start planets.

These results also have implications for our own planet. The Earth, by definition, is located close enough to the star where surface  $CO_2$  ice condensation is impossible under normal circumstances (Figure 3), and it would have been warm so long as the greenhouse effect, including from  $CO_2$ , was potent enough. Nevertheless, the Hadean Earth likely had a  $CO_2$ -rich atmosphere (Kasting 2014), suggesting that it was almost certainly a warm start planet, which may have possibly helped facilitate an early emergence of life.

## 4.2 Comparison with previous work

Although we obtain similar trends, our cold start results differ in certain respects from those of Tabet et al. (2017). In particular, there are discrepancies in the spatial coverage of red (warm planets) and blue (cold and icy displaying surface  $CO_2$  ice) colored areas in Figure 3 between the two studies, which are likely to be mostly attributed to model differences (although there are slight differences in definition of the regions also). In particular, EBMs, such as this one, are quite sensitive to the ice-albedo feedback, and are thus more prone to abrupt transitions between cold and warm climate states (Ramirez & Levi 2018). Our model also employs an atmospheric-ocean heat transport parameterization which likely produces different model behavior than the static ocean assumption made in Tabet et al. (2017).

Another reason for the differences may be in the treatment of clouds. For instance, our  $CO_2$  clouds impact planetary albedo, but they are non-absorbing (see Methods). In contrast, the  $CO_2$  clouds of Tabet et al. (2017) are either radiatively active or inactive across the entire spectrum. Nevertheless, other GCM results are consistent with 1-D results (and, in turn, the EBM results here) in the location of the outer edge of the habitable zone (Wolf 2018). Also, our warm start results agree well with those predicted from 1-D radiative-convective climate models (Kasting et al. 1993; Kopparapu et al. 2013; Ramirez 2018). However, it is unclear how GCMs with fully-coupled atmospheric oceans may compare with the results here. This would be an interesting consideration for future studies.

## 5 CONCLUSIONS

Planets similar to Earth might experience cold or warm stages during the course of their evolution. The carbonate-silicate cycle can stabilize planetary temperatures over geological timescales. While  $CO_2$  generally increases surface temperature, high enough atmospheric  $CO_2$  can trigger atmospheric collapse via  $CO_2$  surface ice condensation (starting at the poles), leading to irreversible glaciation. Such a process could negatively impact the habitability of terrestrial bodies, even if located within the canonical habitable zone. This was argued in Tabet et al. (2017), whom showed that surface  $CO_2$  ice condensation on initially frozen planets orbiting the Sun can significantly reduce the range of habitable orbital distances.

Our work here confirms these results and extends the analysis to rapidly-rotating planets under different starting temperature conditions orbiting a range of star types (F - K). Using a latitudinally-dependent EBM, we show that planets that start out warm can delay surface  $CO_2$  ice condensation to significantly higher  $CO_2$  pressures and larger orbital distances than can cold start (i.e., fully glaciated with  $T_{surf} = 230$  K) planets. This implies a wide habitable zone, consistent with what had been previously computed using simpler 1-D models (Kasting et al. 1993; Kopparapu et al. 2013; Ramirez 2018). Although our model predicts that this zone remains similarly wide across obliquities, we find that inefficient poleward heat transport leads to more surface  $CO_2$  ice production at lower ( $0^\circ$ ) obliquity.

The physics of planetary atmospheres remains complex, particularly for planets unlike the Earth. Future work should continue to use a hierarchy of models to explore the effect of clouds, convection, and the impact that oceans have on the overall heat transport.

## ACKNOWLEDGEMENTS

I.B. acknowledges financial support from the Japanese Ministry of Education, Culture, Sports, Science and Technology (MEXT). R.M.R. acknowledges funding from the Earth-Life Science Institute (ELSI) and from the National Institutes of Natural Sciences: Astrobiology Center (grant number JY310064).

## REFERENCES

- Batalha N. E., Kopparapu R. K., Haqq-Misra J., Kasting J. F., 2016, Earth and Planetary Science Letters, 455, 7
- Caballero R., Langen P. L., 2005, *Geophysical Research Letters*, 32, 1
- Forget F., Hourdin F., Talagrand O., 1998, *Icarus*, 131, 302
- Forget F., Wordsworth R., Millour E., Madeleine J.-B., Kerber L., Leconte J., Marcq E., Haberle R. M., 2013, *Icarus*, 222, 81
- Hoffman P. F., Kaufman A. J., Halverson G. P., Schrag D. P., 1998, *Science*, 281, 1342
- James P. B., North G. R., 1982, *Journal of Geophysical Research: Solid Earth*, 87, 10271
- Kasting J. F., 1991, *Icarus*, 94, 1
- Kasting J. F., 2014, *Geological Society of America Special Papers*, 504, 19
- Kasting J. F., Whitmire D. P., Reynolds R. T., 1993, *Icarus*, 101, 108
- Kirschvink J. L., 1992, *Late Proterozoic low-latitude global glaciation: the snowball Earth*. Cambridge University Press
- Kitzmann D., 2016, *The Astrophysical Journal Letters*, 817, L18
- Kopparapu R. K., et al., 2013, *The Astrophysical Journal*, 765, 131
- North G. R., Coakley Jr J. A., 1979, *Journal of the Atmospheric Sciences*, 36, 1189
- North G. R., Cahalan R. F., Coakley J. A., 1981, Nasa-Cr-177133
- Pierrehumbert R. T., 2005, *Journal of Geophysical Research: Atmospheres*, 110

1  
 2  
 3     8     *I. Bonati and R. Ramirez*  
 4  
 5

- Pierrehumbert R., Abbot D., Voigt A., Koll D., 2011, [Annual Review of Earth and Planetary Sciences](#), 39, 417  
 Ramirez R. M., 2018, *Geosciences*, 8, 280  
 Ramirez R. M., 2020, *Monthly Notices of the Royal Astronomical Society*, 494, 259  
 Ramirez R. M., Kaltenegger L., 2017, *The Astrophysical Journal Letters*, 837, L4  
 Ramirez R. M., Kaltenegger L., 2018, *The Astrophysical Journal*, 858, 72  
 Ramirez R. M., Levi A., 2018, [Monthly Notices of the Royal Astronomical Society](#), 4640, 4627  
 Ramirez R. M., Kopparapu R., Zugger M. E., Robinson T. D., Freedman R., Kasting J. F., 2014, *Nature Geoscience*, 7, 59  
 Rose B. E. J., Cronin T. W., Bitz C. M., 2017, [The Astrophysical Journal](#), 846, 28  
 Soto A., Mischna M., Schneider T., Lee C., Richardson M., 2015, *Icarus*, 250, 553  
 Turbet M., Forget F., Leconte J., Charnay B., Tobie G., 2017, [Earth and Planetary Science Letters](#), 476, 11  
 Vladilo G., Murante G., Silva L., Provenzale A., Ferri G., Ragazzini G., 2013, *The Astrophysical Journal*, 767, 65  
 Williams D. M., Kasting J. F., 1997, *Icarus*, 129, 254  
 Williams D., Pollard D., 2003, [International Journal of Astrobiology - INT J ASTROBIOL](#), 2  
 Wolf E. T., 2018, *Astrophys. J. Lett.*, 855  
 Wordsworth R., Forget F., Millour E., Head J., Madeleine J.-B., Charnay B., 2013, *Icarus*, 222, 1  
 Xu K.-M., Krueger S. K., 1991, *Monthly weather review*, 119, 342  
 Yang J., Abbot D. S., 2014, *The Astrophysical Journal*, 784, 155

This paper has been typeset from a  $\text{\TeX}$ / $\text{\LaTeX}$  file prepared by the author.